FT-IR Spectroscopy: An Advanced Tool for Studying Biomedical Problems

The authors describe several applications of FT-IR spectroscopy in the biomedical sciences, including characterization of healthy and neoplastic human skin samples affected by two kinds of cancers, and examination of liver damage and regeneration caused by carbon tetrachloride, a common environmental contaminant. Results are compared with the morphological analysis by optical microscopy.

Vincenza Crupi, Valentina Venuti and Domenico Majolino

Passing from normal tissue to pathological tissue, cellular biochemistry changes. From a diagnostic and therapeutic point of view, it is fundamental to study the physical and chemical changes occurring in tissues and cells. Many efforts have been made to improve early diagnostic and prognostic methods to better understand the biological nature of diseases. Nowadays, high-resolution techniques permit the adoption of a global approach to the investigation of the initial stages in the transformation processes caused by a pathology, suggesting new and more reliable experiments (1–3).

Many different and complementary experimental techniques have been employed in the medical and pharmacological fields as potential diagnostic tools that can provide, in near real time, information both about the different chemical and morphological structures of healthy and pathological tissues. Most studies have been devoted to light scattering (4–7), including Raman spectroscopy, and fluorescence (8) methods because the response can be obtained quickly with a good signal-to-noise ratio. In particular, among the advanced spectroscopic vibrational methods, Fourier-transform infrared (FT-IR) absorbance represents a good tool in this kind of research (9, 10), providing information concerning the structure and interactions of proteins, lipids, nucleic acids, and so on, both in isolation and in complex assemblies. For example, if compared with positron emission tomography (PET) and magnetic resonance imaging (MRI) scanning methods, well-established techniques for detecting biochemical changes, FT-IR spectroscopy offers the advantage of the lack of external perturbations or large magnetic fields and, of course, the lack of the dependence upon the physical state. Furthermore, FT-IR spectroscopy is able to detect biochemical changes caused by pathologies (11, 12), also at a very early stage of the disease, due to the fact that any biochemical change in the tissue must precede any morphological manifestation of the disease itself. Finally, it gives the opportunity to analyze, in near real time, small samples (less than 1 mm thick and less than 1 cm in diameter), while furnishing reliable and reproducible spectral data (13).

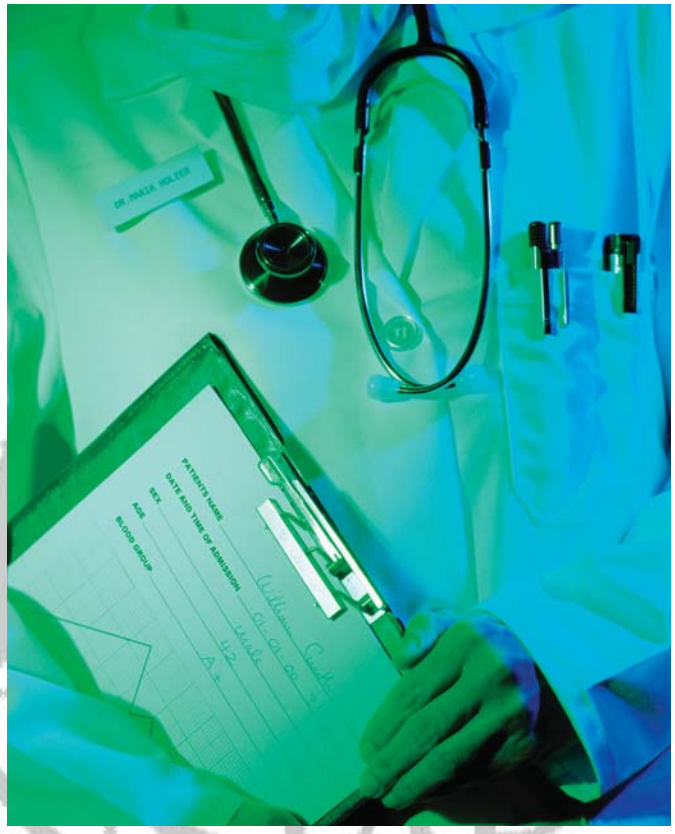

IMAGE COURTESY OF PHOTODISC

In this article, we report the most recent results obtained by our research group, of a detailed study performed by FT-IR spectroscopy together with biochemical analysis and light microscopy, on different kinds of tissues. The aim is to show

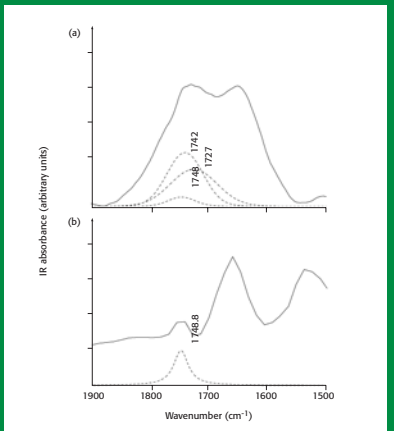

Figure 1. Experimental IR spectra of (a) normal and (b) malignant samples, suffering from epithelioma, together with the main contributions.

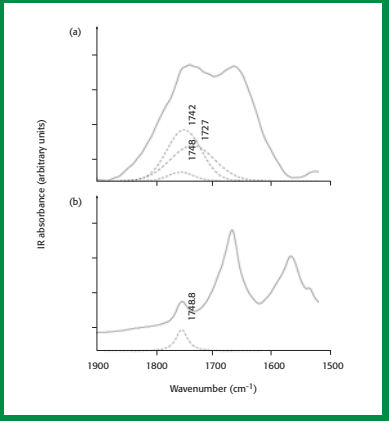

Figure 2. Experimental IR spectra of (a) normal and (b) malignant samples, suffering from basalioma, together with the main contributions.

how the use of infrared spectroscopy can be powerful in studying disease processes.

First we applied FT-IR spectroscopy to normal and neoplastic human skin samples suffering from two kinds of cancer — epithelioma and basalioma. The investigated skin samples were drawn from different parts of the human body, following biopsies. The analysis of the collected IR spectra allowed us to characterize the presence of the pathologies, and to show clear different spectral features passing from the normal tissue to the malignant one particularly within the 1500–2000 cm^{-1} region typical of the lipid bands.

Then we performed a biochemical, structural (by optical microscopy) and dynamical (by FT-IR absorbance) analysis of hepatoxic effects on rat liver, caused by a single administration of carbon tetrachloride (CCl_4) versus the time course. The morphological observations have shown a dramatic increasing of degenerated cellular elements with fatty infiltrations just after 24 h from the CCl_4 treatment and an initial regeneration at 72 h from the CCl_4 treatment. FT-IR spectra of intoxicated samples in the O-H stretching region (3800–3000 cm^{-1}), in the CH stretching region, (3000–2400 cm^{-1}), and in the typical lipids stretching region (1800–1000 cm^{-1}) have shown clear changes interpreted on the basis of the structural and biochemical analysis made on the same samples.

Experimental

Human skin samples were drawn from different parts of the human body after biopsy. In particular, we analyzed a healthy (normal) specimen of skin from the leg, a malignant tissue suffering from basalioma from the forehead, and other malignant samples from the temporal region, respectively, suffering from epithelioma. We obtained thin slides of skin tissue, about 8 µm thick, by cutting the tissues with a freezer microtome (Leica Microsystems, Nussloch, Germany), following a standard routine for morphological studies. The layers were placed successively on KBr pellets that were definitively transparent within the analyzed wavenumber range.

For the rat liver experiments, male Charles River rats weighing 242–325 g were used. Rats were kept under standard conditions, with free access to food and tap water for two weeks before treatment. The animals fasted for 24 h. Liver damage was induced in rats by means of a single intraperitoneal injection of CCl_4,

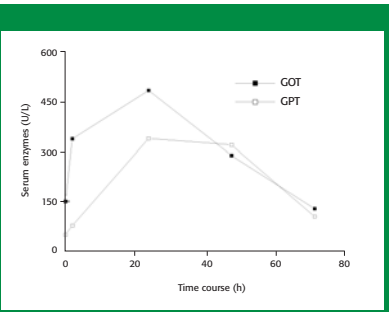

Figure 3. Serum GOT and GPT enzymes plotted vs. CCl_4 time course.

0.3 mL/ kg in olive oil (5 mL/kg). The animals were divided into three groups of five rats each: group 1 received water (5 mL/kg, orally) as normal control; group 2 received vehicle only; group 3 received water and 1 h later was injected with CCl_4. The animals were killed by cervical dislocation under ether anesthesia at 2, 24, 48, and 72 h after CCl_4 administration (14). After blood collection, the blood samples were left to coagulate at room temperature for 1 h. Serum was separated by centrifugation at 3000 rpm and stored at 4 °C for 20 min. Glutamic-oxalacetic aminotransferase (GOT) and Glutamic-pyruvic aminotransferase (GPT) activities were measured using AST/GOT UV-Autom and ALT/GPT UV-Autom test kits (Sentinel CH, Milan, Italy) with an ARCO PC bioanalyzer (Biotechnica Instruments, Rome, Italy). After blood draining, the hepatic tissue was collected quickly from each lobe of the liver and immediately frozen in liquid nitrogen for FT-IR analysis or fixed in 4% paraformaldehyde in 0.2 M phosphate buffer (pH 7.2 ± 7.4), and processed for light microscopy analysis. Morphological changes observed in liver sections were steatosis, fatty change, infiltration of lymphocytes, increase of Kuppfer cell and cells necrosis, and subsequent regeneration. Initially, samples of rat liver from each lobe ~5 mm thick were frozen rapidly in liquid nitrogen and stored at -80 °C until the use. This method allowed us to obtain reliable spectra, preventing the appearance of any unwanted contribution in the analyzed spectral range due to the presence of substances used for fixing. The samples were cut in slides ~30 µm thick by the Leica microtome and laid on KBr pellets. Because of this method, the analyzed samples were quite close to the vital conditions, because no fixing liquid was used, and their homogeneity in the whole extension of the layer allowed us to obtain spectra with high reproducibility.

Experimental FT-IR absorbance data were collected with an ABB Bomem (Zurich, Switzerland) DA8 FT-IR spectrometer working with a globar lamp source, a KBr beamsplitter and a DTGS/KBr detector. For all the cases

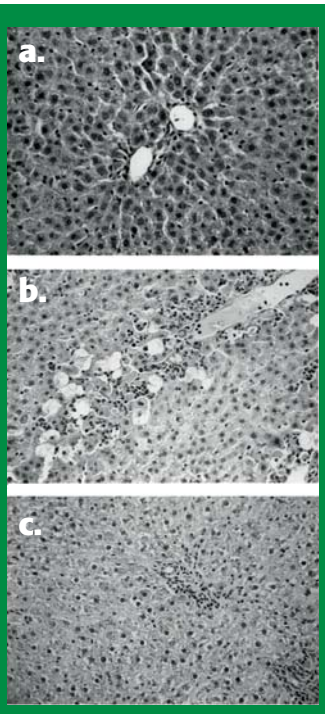

Figure 4. Micrographs (magnification 200x) of (a) normal rat liver and rat liver (b) intoxicated at 24 h and (c) 72 h with CCl_4.

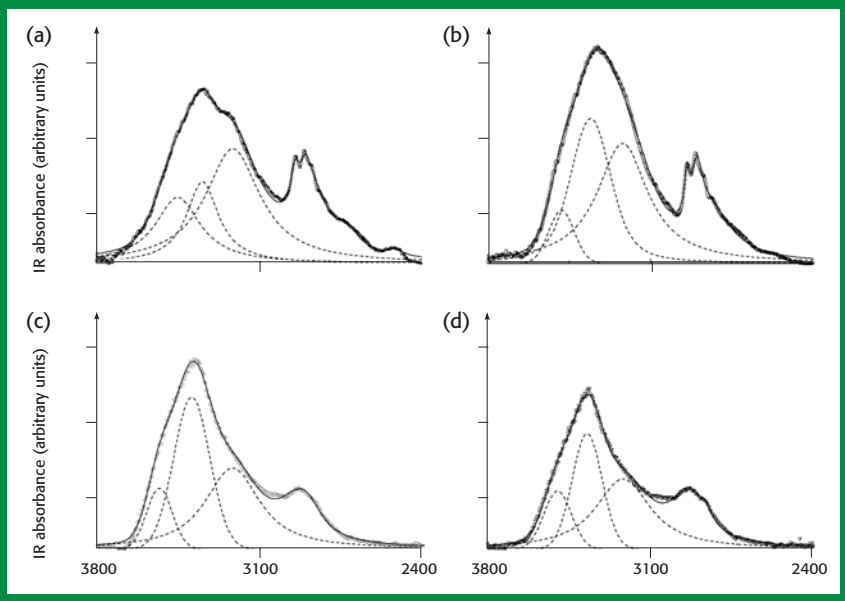

Figure 5. Experimental IR spectra in the O-H stretching region of (a) normal rat liver and rat liver intoxicated at (b) 2 h, (c) 48 h, and (d) 72 h with CCl_4, together with the theoretical best fit (continuous line) and the single components (dashed lines).

under investigation, we used a resolution of 4 cm^{-1}, automatically adding 100 repetitive scans for each run to obtain a good signal-to-noise ratio and high reproducibility in the spectra. Each measurement was repeated several times to ensure the reproducibility of the spectra. First, from all the experimental IR spectra, a baseline was subtracted properly, and then they were normalized to take into account the effective number of absorbers. To account for the hygroscopic character of KBr substrate, we performed absorbance scan on the KBr substrate, before and immediately after the measurements on the samples. In this way, we were sure about the absence of any unwanted wet trace that eventually could affect the analyzed spectral regions. Furthermore, each run was done in dry atmosphere. To check a possible unwanted effect induced by wetting or drying phenomena when dry nitrogen was filled in the sample holder of the FT-IR spectrometer, we compared the IR

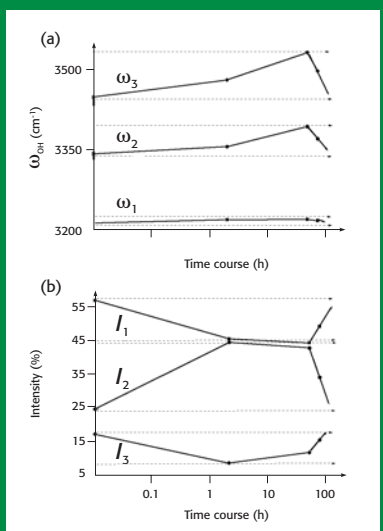

Figure 6. (a) O-H stretching wavenumbers ω_i and (b) percentage intensities I_i plotted as a function of CCl_4 time course. The continuous lines are eye-guides and the dashed ones indicate the normal rat liver parameters.

Table I: Serum GOT and GPT enzyme values as a function of CCl_4 time course.

Group	Number of animals	sGOT	sGPT
Control	5	150.18 ± 12.43	47.13 ± 5.80
Intoxicated, 2 h	5	340.70 ± 0.26	75.43 ± 0.23
Intoxicated, 24 h	5	489.13 ± 64.01	341.80 ± 71.39
Intoxicated, 48 h	5	290.36 ± 82.41	322.20 ± 162.78
Intoxicated, 72 h	5	127.61 ± 40.90	103.53 ± 32.72

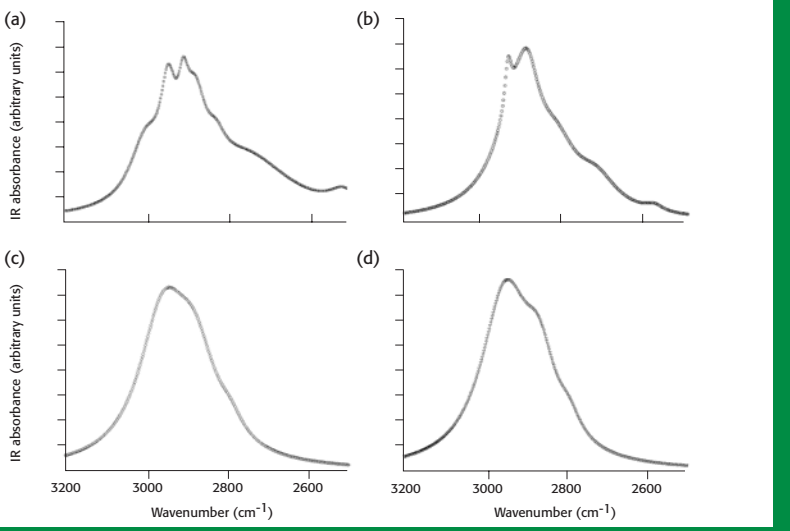

Figure 7. Experimental IR spectra of (a) control and treated rat liver samples after (b) 2 h, (c) 48 h, and (d) 72 h from CCl_4 administration, in the characteristic C-H stretching region.

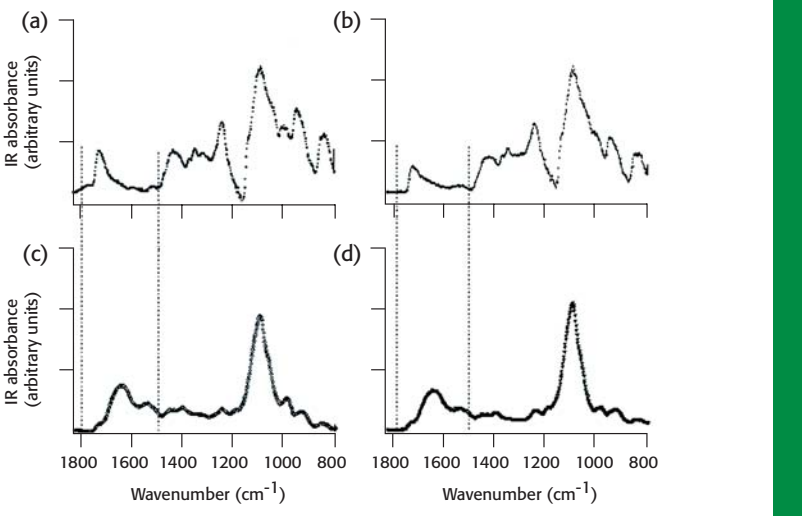

Figure 8. Experimental IR spectra, in the 1800–800 cm^{-1} region, of (a) control and treated rat liver samples after (b) 2 h, (c) 48 h, and (d) 72 h from the CCl_4 administration. The dashed lines mark the most altered region (see text for details).

absorbance spectra of the same sample both in presence and in absence of air. The resulting IR spectra do not show significant differences.

Results and Discussion

Human skin consists of three main layers: epidermis, dermis, and subcutis (14). The thickness of each layer depends upon the particular region of the body, the age and the gender. The epidermis is made up of epithelial tissue and is rich in keratinocytes that provide keratin. Its vibrational spectrum essentially is characterized by the typical bands of the proteins. The dermis is made up of connective tissue and hence mainly of collagen type I, whose main component is a fibrous protein. In fact, the vibrational features of the dermis are similar to those of this kind of collagen. Finally, the vibrational spectral profile of the subcutis is related strictly to those of lipids with the characteristic band centered at about 1750 cm^{-1}, typical of the C=O vibration. The variations observed in the spectra usually reflect changes in the structure due to the presence of the cancer, but it also is necessary to take

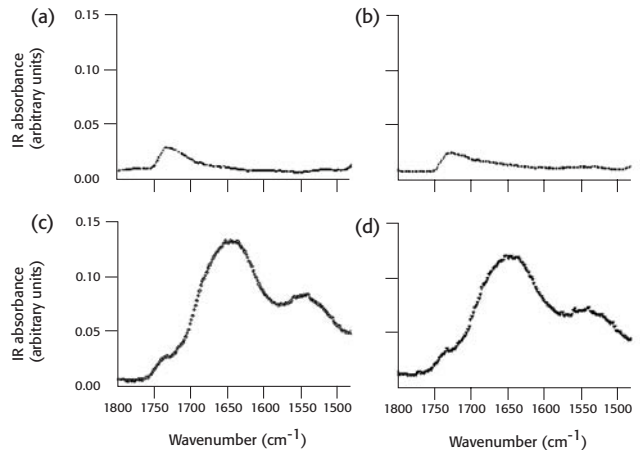

Figure 9. Experimental IR spectra of (a) control and treated rat liver samples after (b) 2 h, (c) 48 h, and (d) 72 h from the CCl_4 administration, in the wavenumber range typical of lipids stretching (1800–1500 cm^{-1}).

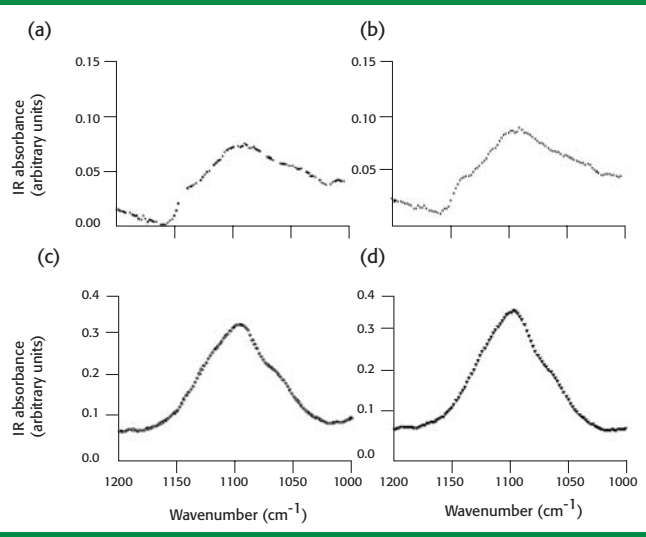

Figure 10. Experimental IR spectra of (a) control and treated rat liver samples after (b) 2 h, (c) 48 h, and (d) 72 h from the CCl_4 administration, in the wavenumber range typical of phosphate stretching (1200–1000 cm^{-1}).

other factors into account. As an example, the amount of lipids depends upon many parameters: race, age, food, and part of the body. These, together with the high molecular and chemical complexity of the tissue, make the full characterization of the tissue very hard. Therefore, a correct band assignment requires a deep knowledge of the tissue components. However, there are three common constituents of human tissue: cellular membranes, proteins and nucleic acids.

We studied the spectral region from 1500–2000 cm^{-1}, which appears involved particularly in the changes caused by the presence of cancers. The experimental spectra of all the analyzed samples were normalized properly and deconvoluted into Lorentzian profiles. By comparing the normal control sample spectra with the pathological ones, we obtained information on the bands of the main components that presented a frequency shift or even disappeared. The studied spectral region is characterized mainly by the presence of proteins (amide I and II), many aminoacids, water, lipids of cellular membranes, and phospholipids. Figure 1 shows the IR absorbance spectra of the normal control sample and the malignant one, suffering from epithelioma, drawn from the temporal region. From the band deconvolution, the main changes can be attributed to the following sub-bands, centered at 1727 and 1742 cm^{-1} (C=O vibration of cellular membrane lipids), and at 1748 cm^{-1} (C=O vibration of phospholipids). Upon inspection of Figure 1, it is clear that the three above-mentioned sub-bands are present only in the normal specimen (Figure 1a), while in the pathological case (Figure 1b) the two contributions owing to the cellular membranes have disappeared. The same occurrence seems to take place in the case of the tissue suffering from basalioma (see Figure 2a and 2b). The change in the intensity of the band, centered at 1748 cm^{-1}, essentially could be due to the amount of fat in the different analyzed specimen of human tissue, as it can be seen in the absorbance spectra.

With the rat liver samples, the investigation was addressed to show the effectiveness of the employed experimental techniques, by monitoring the structural changes that lead the human liver to cellular death that is caused by chemical agents. In the analyzed samples, these toxic effects were provoked by the administration of CCl_4. In fact, the pathology induced by this solvent experimentally reproduces a good model for biochemical, morphological and clinical studies.

CCl_4 is one of the most studied solvents in hepatic disease (15–18), because it is one of the most diffuse environmental contaminants, widely used as a cleaning agent and grain fumigant. In addition, in drinking water supplies, main sources of CCl_4 and other volatile organic compounds are given by emission from product manufacturing and leakage from storage tanks. This solvent, even at low levels, causes reversible lesions in the liver of all the subjects exposed at certain doses, and the causes are reproducible in the animals. The acute pathology by CCl_4 usually shows accumulation of lipids (steatosis and fatty infiltration) leading to cellular death (necrosis). Hepatic disease already is evident after a single administration of CCl_4 since the first hour, as shown by transmission electronic microscopy (TEM) (19). In fact,

Table II: Sub-bands center frequencies ω_i and relative intensities I_i for rat liver vs. CCl_4 time course.

Rat liver	ω_1 (cm^{-1})	ω_2 (cm^{-1})	ω_3 (cm^{-1})	I_1 (%)	I_2 (%)	I_3 (%)
Normal	3213.6	3344.1	3451.0	57.3	25.1	17.6
Intoxicated, 2 h	3220.0	3357.8	3483.6	45.9	44.9	9.1
Intoxicated, 48 h	3220.6	3395.7	3535.0	44.7	43.2	12.2
Intoxicated, 72 h	3218.2	3372.9	3500.3	49.6	34.5	15.9

active oxygen species play a critical role in the alteration of cellular functions and cell death. CCl_4 activates free radicals metabolically by cytochrome P450 in the cisternae of endoplasmic reticulum of hepatocytes. The morphological change of endoplasmic reticulum is evident only by ultrastructural observations. In addition, non-lethal doses of CCl_4 induce balanced effects between cell necrosis and hepatic regeneration (20, 21).

Biochemical measurements. It is well known that the hepatic alteration by chemical agents can irreversibly damage the activity of enzymes which are devoted to biotransformation processes (22). So the determination of their activity is one of the most useful tools in the study of hepatoxicity. The biochemical effects obviously are correlated to the seriousness of the damage. The results, coming from our biochemical measurements and obtained in the case of CCl_4-treated rats, show a significant increase of serum GOT and GPT enzymes at 24 h with respect to the control group, persisting until 48 h. They also show a decrease of these values at 72 h after administration. The data summarized in Table I are shown in Figure 3. The increasing of these enzymatic activities showed a clear cellular alteration and the loss of functional integrity of cellular membrane of hepatocytes (23).

Light microscopy measurements. Morphological observations of rat liver, 2 h after CCl_4 treatment, did not show any significant change if compared with the normal one (see Figure 4a). Steatosis, fatty change, infiltration of lymphocytes, increased Kuppfer cells, and cell necrosis are conspicuous in liver samples after 24 h (Figure 4b) following treatment. These features remained stable until 48 h after treatment. At 72 h after treatment (Figure 4c), all damage patterns have almost disappeared. Moreover, cell proliferation was evident in hepatic lobule.

FT-IR absorbance measurements. Taking into account the previous structural results obtained by biochemical measurements and light microscopy, we assigned and interpreted, first of all, the sub-bands present in the IR absorbance spectra in the CH-OH stretching range (3800–2400 cm^{-1}).

In the spectra of all the samples, we distinguished two clear regions: the first one spreads from 3000 cm^{-1} to 2400 cm^{-1} and it is characteristic of the C-H stretching mode with different symmetries (CH_2, CH_3, and so forth). The second one spreads from 3800 cm^{-1} to 2900 cm^{-1}, and it is characteristic of the O-H stretching vibration. The observed variations in the C-H stretching band profiles could be originated by the presence of new molecular groups containing C-H units caused by steatosis. As far as the spectral region from 3800 cm^{-1} to 3000 cm^{-1} is concerned, we took into account the absorbance contributions due to the N-H stretching from amide band, centered at about 3300 cm^{-1} and 3500 cm^{-1}, and typical in cellular proteins besides the characteristic OH stretching vibrations. The former bands actually play a minor role because they are hidden by the more intense O-H stretching vibrations. Moreover, because we followed the time evolution of O-H bands, this contribution was almost constant in time, hence did not influence the O-H stretching band.

For H-bonded systems, the existence of various local minima in the system potential energy generally is associated with the change in the $R_{O–O}$ distances (24, 25). It is therefore possible to explain the spectral variations of the O-H stretching vibration, spreading over a large ω-range, 3000–3800 cm^{-1}, and dramatically changing in frequency (red shift) and intensity with respect to the original narrow O-H band centered at ~3630 cm^{-1}.

Hence the experimental IR data, first normalized for the C-H stretching area, were deconvolved into symmetrical profiles (Figures 5a–d) having a wavenumber shift with respect to the fundamental free O-H stretching vibration. Table II shows the best-fit parameters versus CCl_4 time course. In order to interpret the complex IR spectra obtained, we took into account that in our specimens the O-H stretching band contained both vibrations induced by water involved in intracellular bonds and water involved in Coulombian bonds with O-H groups (centered at about 3350 cm^{-1}, from literature) (26), probably belonging to fatty changes of hepatocytes.

To best fit the O-H stretching region, we fitted the C-H vibrational range as well. Hence, in normal rat liver, the best-fit procedure led to the presence of three different contributions (Table II): the first one (centered at ω_1 = 3216.1 cm^{-1}) is related to O-H vibrations of tightly bonded H_2O molecules, the second one (ω_2 = 3344.1 cm^{-1}) could be connected strictly to the O-H groups due to metabolic processes, and the third one (ω_3 = 3451.0 cm^{-1}) is due to O-H vibrations belonging to H_2O molecules strongly distorted by asymmetric bonds. After CCl_4 administration, we observed a clear evolution in the O-H stretching band starting from 2 h. Figures 6a and 6b show the wave numbers (ω_1, ω_2, ω_3) and the behavior of the relative intensities (I_1, I_2, I_3) versus carbon tetrachloride time course, respectively. The first point at t = 0 h represents the normal state of liver, i.e. before CCl_4 administration, and the dashed lines mark the healthy state. A noteworthy result can be obtained from the relative intensities, I_i (i = 1, 2, 3) plot versus the time course that also can confirm the above assignment of the subbands. In fact, at first I_1 (tightly bonded water) and I_3 (distorted water) values, both related to intracellular H_2O (or bulk water), tend to decrease, after (48 h from the treatment) we observe a subsequent increasing. I_2 shows the opposite trend that can be due to the lipidic peroxidation process, which is the typical damage that fatty acids suffer from CCl_4 in the early stage just after 2 h from the treatment. We have to emphasize that this last important result can be revealed by TEM and biochemical analysis as well, but not by light microscopy. The above behavior, which strongly recalls the evolution of GOT and GPT enzymes values (see Figure 3),

agrees with the real destruction of the cells due to CCl_4 administration that leads to the disappearance of intracellular water in relation with the peroxidation processes. Furthermore, the occurrence that the number of O-H groups increases because of steatosis and fatty infiltration is connected strictly with the initial increasing of I_2. This behavior reflects the light microscopy results exactly. The effect of liver regeneration is evident starting after 48 h from CCl_4 treatment; in fact, in this region the data show a clear trend to restore the state typical of normal liver and to a complete restitutio ad integrum of the parenchyma.

Figure 7 reports the experimental IR spectra starting from the control specimen (Figure 7a) to the 72-h treated specimen (Figures 7b–d) in the above mentioned wavenumber range. The C-H stretching vibrations that give rise to the strongest bands in the spectra of lipids with the CH_2 antisymmetric and symmetric stretching modes at about 2920 and 2850 cm^{-1}, respectively, clearly appear altered because of the treatment process with CCl_4. An initial restoration of the healthy condition seems to appear after 72 h from the solvent administration, as it is evident from the partial restoration of the well-defined peaks typical of normal conditions.

Taking into account the above mentioned results, we tried to explain the FT-IR spectral features in the stretching region of the lipids as well. Figure 8 shows the IR absorbance spectra for all the investigated samples in the wavenumber range (1800–800 cm^{-1}). As we can see from an inspection of the figure, the most relevant changes in the spectral profile are evident in the 1800–800 cm^{-1} range, passing from the control sample, (Figure 8a), to the treated ones (Figures 8b–d). The dashed lines include the spectral region affected mostly by the hepatic damage. In Figure 9 we reported in particular the FT-IR spectra in the 1800–1500 cm^{-1} region. The large bands due to the C-O and C=C stretching of lipids centered at about 1540 cm^{-1} and 1650 cm^{-1}, respectively, are absent in the normal liver tissue. They start to appear after 2 h from the CCl_4, becoming increasingly evident after 48 h and 72 h. This occurrence can be explained taking into account that one of the worst damages induced by the CCl_4 administration is the fatty infiltration, which is one of the causes for the formation of the steatosis, as has been revealed already by our biochemical and light microscopy results. Another group of infrared bands characteristic of phospholipids (26) (see Figure 10) that originates from the vibrations of phosphate moiety is centered at ~1085 cm^{-1} and is due to the double bond P=O stretching (PO_2 antisymmetric and symmetric stretch, respectively). This large band displays a higher intensity in the treated rat liver samples and appears sharper than in the case of the control specimen. This spectral evidence could confirm the alteration caused by CCl_4 that originates the formation of fat in the liver.

Conclusion

In this paper, we presented the main results of a detailed spectroscopic analysis performed by our research group on many kinds of tissues representative of different biomedical problems.

First, we performed a spectroscopic study on normal and malignant skin samples to show how powerful the use of infrared spectroscopy can be in studying disease processes. The comparison between the normal specimen and the malignant one has shown that the lipids of cellular membranes are the most involved in the structural changes resulting from the presence of the two kinds of studied cancers — epithelioma and basalioma.

Our work then has been addressed to characterize, by the employment of coupled different methods, the hepatotoxic damage in rat liver caused by carbon tetrachloride administration and its further regeneration. With the support of the biochemical and structural results obtained, it is clear that the FT-IR absorption technique provided reliable, reproducible spectra, which could be used to distinguish normal and injured specimens unambiguously.

In particular, it was clear that earlier injuries of liver parenchyma due to CCl_4 treatment, starting from 2 h, already were evident by FT-IR analysis in all the analyzed wavenumber regions. This damage reflectes the variation in the intensities of the bands of the lipids both at low and at high frequency, in agreement with the typical morphological and biomedical alterations of the liver in presence of steatosis. Furthermore, FT-IR spectroscopy was able to verify the start of the hepatic regeneration after about 48 h from CCl_4 treatment.

It is worth emphasizing that, when compared with other analytical experimental techniques, FT-IR absorbance furnishes a spectroscopic analysis with the advantages of a fast characterization, a good reproducibility of the experimental data, and the possibility of examining unfixed samples with reduced dimension. The present state of the art warrants good chances of success in improving the methods of medical diagnostics by FT-IR spectroscopy.

References

1. D.M. Haaland, H.D.T. Jones, and E.V. Thomas, *Appl. Spectrosc.* **51**, 340 (1997).
2. E. Debenedetti, L. Deodori, M.L. Trinca, P. Vergatini, F. Salvati, F. Mauro, and G. Spremolla, *Appl. Spectrosc.* **44**, 1276 (1990).
3. P.T.T. Wong and B. Rigas, *Appl. Spectrosc.* **44**, 1715 (1990).
4. Mahadevan-Jansen and R. Richards-Kortum, *J. Biom. Optics* **1**, 31 (1996).
5. Y. Ozaki, *Appl. Spectrosc. Rev.* **24**, 259 (1988).
6. S. Nie, K. Bergbauer, J. Ho, J. Kuck, and N. Yu, *Spectroscopy* **5**, 24 (1990).
7. B. Schrader, S. Keller, T. Loechte, S. Fendel, D. Moore, A. Simon, and J. Sawatzki, *J. Mol. Struct.* **348**, 293 (1995).
8. C. Liu, B. Das, W. Akins, S. Lubicz, J. Cleary, R. Prudente, E. Celmer, A. Caron, and R. Alfano, *J. Photochem. Photobiol. B: Biol.* **16**, 187 (1992).
9. M. Jakson and H.H. Mantsch, in *Advances in Infrared and Raman Spectroscopy*, R.J.H. Clark and R.E. Hester, Eds. (Wiley, Hayden, 1996), pp. 185–215.
10. D. Neumann, C.P. Schultz, and D. Helm, in Infrared Spectroscopy of Biomolecules, H.H. Mantsch and D. Chapman, Eds. (Wiley-Liss, New York, 1996), pp. 279–310.
11. P T.T. Wong, K. Wong and M.F.K. Fung, *Appl. Spectrosc.* **47**, 1058 (1993).
12. V. Crupi, S. Galli, D. Majolino, P.

Migliardo, S. Pergolizzi, and V. Venuti, *Spectroscopy — An International Journal* **16**, 245 (2002).
13. V. Crupi, D. Majolino, P. Migliardo, M.R. Mondello, M.P. Germanò, and S. Pergolizzi, *Vibrational Spectroscopy* **25**, 213 (2001).
14. B. Schrader, B. Dippel, S. Fendel, R. Freis, S. Keller, T. Löchte, M. Riedl, E. Tatsch, and P. Hildebrandt, *Infrared Spectroscopy: New Tool in Medicine* **66**, 3257 (1998).
15. H.J. Kim, J.V. Bruckener, C.E. Dallas, and J.M. Gallo, *Toxicol. Appl. Pharmacol.* **102**, 50 (1990).
16. H.J. Kim, S. Odend'hal, and J.V. Bruckener, *Toxicol. Appl. Pharmacol.* **102**, 34 (1990).
17. U.Y. Sanzgiri, H.J. Kim, S. Muralidhara, C. E. Dallas, and J.V. Bruckener, *Toxicol. Appl. Pharmacol.* **134**, 148 (1995).
18. U.Y. Sanzgiri, V. Srivatsan, S. Muralidhara, C.E. Dallas, and J.V. Bruckener, *Toxicol. Appl. Pharmacol.* **143**, 120 (1997).
19. M. Mori, *Acta Pathos. Jpn.* **33**, 911 (1983).
20. P.S. Rao, R.S. Mangipudy, and H.M. Mehendale, *Toxicology* **118**, 181 (1997).
21. N. Sanz, C. Diez-Fernandea, A.M. Alvarez, L. Fernandez-Simon, and M. Cascales, *Toxicol. Appl. Pharmacol.* **154**, 40 (1999).
22. G.L. Plaa and M. Charbonneau, in *Principles and Methodology of Toxicology*, A. Wallace Hayes, Ed. (Raven, New York, 1994), p. 389.
23. S. Premila, G. Wilferd, and R. Banumathi, *Biochem. Biophys. Acta* **1362**, 169 (1997).
24. D. Hadzi and S. Bratos, in *The Hydrogen Bond I*, P. Shuster, G. Zundel and C. Sandorfy, Eds. (North-Holland, Amsterdam, 1976), p. 565.
25. S. Bratos, in S. Bratos, and F. Pick, Eds., *Vibrational Spectroscopy of Molecular Liquids and Solids* (Plenum Press, New York, 1980), p. 43.
26. H. L. Casal and H. Mantsch, *Biochem. Biophys. Acta* **779**, 381 (1984). ■

Vincenza Crupi, Valentina Venuti and **Domenico Majolino** are professors at Messina University, Department of Physics (Messina, Italy).
E-mail: Vincenza.Crupi@unime.it.